Structure and Crystallization of Alkaline-Earth Aluminosilicate Glasses: Prevention of the Alumina Avoidance Principle

Amarnath R. Allu,[a,#,*] Anuraag Gaddam,[b,#] Sudheer Ganisetti,[c] Sathravada Balaji,[a] Renée Siegel,[d] Glenn C. Mather,[e] Margit Fabian,[f] Maria J. Pascual,[e] Nicoletta Ditaranto,[g] Wolfgang Milius,[h] Jürgen Senker,[d] Dmitrii A. Agarkov,[i,j] Vladislav. V. Kharton,[i] José M. F. Ferreira,[b*]

[a] Glass Division, CSIR-Central Glass and Ceramic Research Institute, 700032, Kolkata, India
[b] Department of Materials and Ceramic Engineering, CICECO, University of Aveiro, 3810–193 Aveiro, Portugal
[c] Department of Materials Science and Engineering, Institute I, Friedrich-Alexander-Universität Erlangen-Nürnberg, Martensster. 5, 91058 Erlangen, Germany
[d] Inorganic Chemistry III, University of Bayreuth, 95440 Bayreuth, Germany
[e] Instituto de Cerámica y Vidrio (CSIC), C/Kelsen 5, Campus de Cantoblanco, 28049 Madrid, Spain
[f] Centre for Energy Research, 1121 Budapest Konkoly-Thege st. 29-33, Hungary
[g] Dipartimento di Chimica e Laboratorio di Diagnostica Applicata ai Beni Culturali, Università degli Studi di Bari "Aldo Moro", via Orabona 4, 70125 Bari – Italy
[h] Inorganic Chemistry I, University of Bayreuth, 95440 Bayreuth, Germany
[i] Institute of Solid State Physics RAS, 142432 Chernogolovka, Moscow District, Russia
[j] Moscow Institute of Physics and Technology, Institutsky lane 9, Dolgoprudny 141700, Moscow District, Russia

ABSTRACT: Aluminosilicate glasses are known to follow Al-Avoidance principle, which states that Al–O–Al linkages are energetically less favourable. Therefore, as long as there is a possibility for Si–O–Al linkages to occur in a glass composition, Al–O–Al linkages are not formed. The current paper shows that breaching of the Al-Avoidance principle is essential for understanding the distribution of network-forming AlO_4 and SiO_4 structural units in alkaline-earth aluminosilicate glasses. The present study proposes a New Modified Random Network (NMRN) model, which accepts Al-O-Al linkages, for aluminosilicate glasses. The NMRN model consisting of two regions, a network structure region (NS-Region) composed of well separated homo-nuclear and hetero-nuclear framework species and a channel region (C-Region) consisting of non-bridging oxygens (NBOs) and non-framework cations. The NMRN model accounts for the structural changes and devitrification behaviour of aluminosilicate glasses. A parent Ca- and Al-rich melilite-based $CaO–MgO–Al_2O_3–SiO_2$ (CMAS) glass composition was modified by substituting MgO for CaO and SiO_2 for Al_2O_3 to understand variations in the distribution of network-forming structural units in the NS-region and devitrification behaviour upon heat treating. The structural features of the glass and glass-ceramics (GCs) were meticulously assessed by advanced characterization techniques including neutron diffraction (ND), powder X-ray diffraction (XRD), ^{29}Si and ^{27}Al magic angle spinning (MAS)-nuclear magnetic resonance (NMR), and *in-situ* Raman spectroscopy. ND revealed the formation of SiO_4 and AlO_4 tetrahedral units in all the glass compositions. Simulations of chemical glass compositions based on deconvolution of ^{29}Si MAS-NMR spectral analysis indicate the preferred formation of Si–O–Al over Si–O–Si and Al–O–Al linkages and the presence of a high concentration of non-bridging oxygens leading to the formation of a separate NS-region containing both SiO_4 and AlO_4 (Si/Al) (hetero-nuclear), in addition to the presence of $Al_{[4]}$-O-$Al_{[4]}$ bonds; this region co-exists with a predominantly SiO_4-containing (homo-nuclear) NS-region. In GCs, obtained after heat treatment at 850 °C for 250 h, the formation of crystalline phases, as revealed from Rietveld refinement of XRD data, may be understood on the basis of the distribution of SiO_4 and AlO_4 structural units in the NS-region. The *in-situ* Raman spectra of the GCs confirmed the formation of a Si/Al structural region, as well indicating interaction between the Al/Si region and SiO_4-rich region at higher temperatures, leading to the formation of additional crystalline phases.

1. INTRODUCTION

Research on aluminosilicate glass and glass-ceramic (GC) materials is of special interest owing to their many potential uses in photonics, optoelectronics, sealing, and biomedicine.[1-6] Aiming at broadening the scope of their technical applications, binary, ternary and multi-component systems have been investigated.[1-5] The capability of aluminosilicates to accept a wide range of oxides makes them very attractive for designing materials with tailor-made properties for specific applications.[7-9] When developing new glass materials by performing systematic changes in the chemical composition, it is necessary to define the non-crystalline structure of the primary glass and fluctuations occurring with changes in the composition in order to control the macroscopic properties. To this end, the use of suitable tools to assess the structural details and a specific structural model are required. MAS NMR and Raman spectroscopy along with molecular dynamics simulations have contributed greatly to the understanding of glass structure.[10-14] In addition to MAS NMR and Raman spectroscopy that have limitations for alkaline-earth cations,[15,16] neutron-diffraction techniques can provide interatomic distance and information on the the coordination distribution,[12] including alkaline-earth cations, in aluminosilicate-based glasses and GCs. Therefore, a suitable combination of structural tools is essential to properly assess the structure of glass materials.

Moreover, a deeper fundamental understanding of the structure also assists in scrutinizing the growth mechanism of crystalline phases, which is another crucial aspect towards developing tailor-made GC materials for specific applications. For example, the influence of Sr substitution for Ca on the silicate network structure of diopside-based glasses was previously investigated by correlating the glass composition with structural data gathered by various experimental techniques, illustrating that a thorough understanding of the structure and crystallization behaviour of glasses can accelerate the discovery and improvement of materials for relevant applications.[7] Diopside was shown to crystallize homogeneously at lower levels of Sr substitution for Ca (up to 30 mol%); greater Sr contents favoured the heterogeneous crystallization of akermanite phase. The formation of Mg^{2+}–O_4 tetrahedral units at higher Sr contents and the presence of highly-mobile, isolated Si^{4+}–O_4 tetrahedral units accounted for the observed changes in the crystallization mechanism.[7]

Data reported on aluminosilicate glasses over the last century describing composition-structure-property relationships that are not yet fully understood.[7-20] This is mainly due to the distinct possible roles played by the glass constituents, including intermediate oxides such as MgO in some special cases,[4] and network modifiers. The intermediate oxides, especially alumina, play a critical role in constructing the network structure of glass materials owing to the possibilities for the formation of variable coordination states (AlO_4, AlO_5 and AlO_6). In this respect, the "Loewenstein Al avoidance rule"[21] assumes that direct $Al_{[4]}$–O–$Al_{[4]}$ linkages are absent and the excess negative charge of an $[AlO_4]^-$ tetrahedron is counterbalanced by charge compensating ions, excluding NBO species. However, the currently available theories poorly describe the structural experimental data for aluminosilicate glasses. Considering these limitations and within the framework of the modified random network (MRN) model,[22] Moesgaard et al. have investigated the distribution of structural units at intermediate-range order for peralkaline calcium aluminosilicate (CAS) glasses by proposing a Quasi-Heterogeneous intermediate-range order (QH-IRO) model.[13] According to the QH-IRO model, clustering of NBOs results in highly polymerized regions of alternating SiO_4 and AlO_4 tetrahedra as well as highly depolymerized regions with only minor Al contents. This model mainly considers the presence of specific $Q^n(mAl)$, where n (ranging from 0 to 4) is the number of bridging oxygens (BOs) associated with Si and m (ranging from 0 to 4) is the number of Al in the next-nearest neighbour (NNN) of Si tetrahedron, structural units (for n=4, m=0 and 4; for n=3, m=0 and 3; for n=2, m=0 and 2; for n=1, m=0; and for n=0, m=0) instead of considering all 15 different possible structural units in aluminosilicate glasses. Although application of the QH-IRO model well defines the structure and crystallization behaviour of CAS glasses, it mainly limits the structural units to those existing in aluminosilicate glasses. Nevertheless, especially in the presence of a high concentration of network modifier cations, the possibility for the existence of $Q^4(3Al)$, $Q^4(2Al)$, $Q^4(1Al)$, $Q^3(2Al)$, $Q^3(1Al)$ and $Q^2(1Al)$ units in aluminosilicate glasses should not be discounted while explaining the fraction of Al in Al-O-Al bonds in accordance to the ^{27}Al MAS-NMR experimental spectra for CAS glass system.[13,23,24] In general, the [27]Al chemical shift for Al in Al(4)-O-Al(4) is usually between 70 to 80 ppm, which is slightly higher (about ~10 ppm) than that for Al in Al(4)-O-Si(4) units. This indicates that ^{27}Al MAS-NMR spectra were unreliable to be used for quantitative analysis, so they were only used qualitatively. New models should, therefore, be proposed after thorough investigation to explain the distribution of structural units and network structure of alkaline-earth-containing aluminosilicate glasses.

In view of the above, we have attempted to explain the distribution of structural units in aluminosilicate glass network structure based on proposing a new modified random network (NMRN) model, considering the breakdown of the Al-avoidance principle and the existence of all possible structural units, within the framework of the MRN model. The Löewenstein's rule of "aluminium avoidance"[21] is commonly assumed while understanding the distribution of AlO_4 and SiO_4 structural units in framework aluminosilicates,[25,26] since the rule was conceptualised in 1954.[21] In general, this rule proposes that Al-O-Si linkages are more favourable than the Al-O-Al and Si-O-Si linkages in crystals of silicates and aluminates. This rule is also proved by several theoretical calculations.[27,28] Nevertheless, there have been few suggestions that violation of this rule is possible, especially in alkaline-earth aluminosilcate glasses.[27,29] Therefore, violation of this rule is considered essentially in the present study

to explain the distribution of AlO_4 and SiO_4 structural units in NS-region based on NMRN model in CMAS modified glasses. According to the MRN model, proposed by Greaves,[22] the glass network consists of a network structure region (NS-Region) composed of framework species connected by bridging oxygens (BOs) and a channel region (C-Region) composed of non-bridging oxygens (NBOs) and non-framework cations (e.g., network-modifier cations). Schematic illustrations of a network structure and channel region in a plane are presented in references 22 and 30. The NMRN model assumes that the NS-region in the MRN model consists of well-separated clusters of homonuclear and heteronuclear framework species. The NMRN model is proposed mainly based on the following two considerations. In view of the fact that [29]Si chemical shifts are highly sensitive to the type of tetrahedral unit (either AlO_4 or SiO_4) present in the second coordination sphere of SiO_4 tetrahedra and the number of non-bridging oxygens attached to the SiO_4 tetrahedra,[31,32] a deconvolution of ^{29}Si MAS NMR spectra reveal the concentrations of various structural units present in the NS-region of the glass structure. Simulations of the chemical compositions from the results of deconvolution of ^{29}Si MAS NMR spectra, considering the possibilities for Si-O-Si, Si-O-Al and Al-O-Al linkages to match with the experimentally designed chemical compositions, reveal the distribution of structural units in the NS-region of the aluminosilicate glass structure.

Table 1: Chemical compositions and cation–oxygen distances corresponding to cation–oxygen partial atomic-pair correlation functions displayed in Fig. S1 obtained from RMC modelling of the parent and modified CMAS glasses.

Chemical compositions of glasses (mol %)				
	CaO	MgO	Al_2O_3	SiO_2
CMAS-M0[32]	38.7	9.7	12.9	38.7
CMAS-M1	33.7	14.7	7.9	43.7
CMAS-M2	28.7	19.7	2.9	48.7
Peaks from pair correlation function, $g_{i-O}(r)$ (Å)				
	Ca–O	Mg–O	Al–O	Si–O
CMAS-M0	2.35 (±0.02Å)	1.70 (±0.02Å)	1.75 (±0.01Å)	1.6 (±0.01Å)
CMAS-M2	2.30 (±0.02Å)	1.70 & 2.15 (±0.02Å)	1.75 (±0.01Å)	1.62 (±0.02Å)

In the present study, a parent glass composition, CMAS-M0[32,33] was modified by substituting Mg for Ca and Si for Al to obtain the compositions labelled as CMAS-M1 and CMAS-M2, presented in Table 1, where M1 and M2 represent the level of modification. The total concentrations of network modifers and network formers were kept fixed to observe the changes in distribution of structural units in the NS region. The SiO_2 and Al_2O_3 concentrations were changed to observe the variation in the percentages of Al in Al-O-Al bonds whereas; MgO concentration was increased over CaO to observe the variation in coordination of Mg. The structure of these glasses and GCs were thoroughly studied by employing neutron diffraction (ND), *in-situ* X-ray diffraction, [29]Si and [27]Al magic angle spinning (MAS) NMR spectroscopy, and in-situ Raman vibrational spectroscopy. The structural information obtained from these complementary techniques was employed to explain the crystal growth mechanism on heat-treating glasses at 850 °C for 250 h.

2. EXPERIMENTAL

The detailed synthesis procedure of the glass and GCs is described eleshewhere.[33] The glass powders with mean particle size between 10 and 15 µm were pressed uniaxially (80 MPa) to form rectangular bars with dimensions of 4 mm × 5 mm × 50 mm. The GCs were produced after sintering the rectangular glass powder compacts at 850 °C for 250 h in air with a heating rate of 5 K min⁻¹. Neutron powder diffraction (ND) measurements were performed at the 10 MW Budapest research reactor using the two-axis 'PSD' diffractometer (monochromatic wavelength was λ_0 = 1.068 Å);[34] the detailed experimental procedure including Reverse Monte Carlo (RMC) modelling is provided elsewhere.[32] X-ray powder diffraction data were collected using a Philips PW3710 high-resolution diffractometer. Refinement was carried out with the Fullprof software[35] using interpolation of points to model the background. ^{27}Al solid-state NMR experiments were acquired on a Bruker Avance-III HD operating at a B0 field of 14.1 T. ^{29}Si MAS NMR spectra were recorded on a Bruker Avance-II spectrometer operating at 7.1 T ([29]Si frequency at 59.62 MHz) using a 7 mm probe at a spinning rate of 5 kHz. In-situ Raman spectra were obtained using a Horiba LabRam HR 800 Evolution confocal Raman microscope, with a 532 nm excitation laser and a 100× objective lens (NA = 0.9). All spectra for glass-ceramics were recorded in the range 200–1200 cm⁻¹ with an integration time of 1 s and 3 accumulations per spectrum on increasing the temperature from 100 to 800 °C at an interval of 100 °C. Detailed experimental procedure related to ND, XRD, MAS NMR and *in-situ* Raman is provided as SI.

3. RESULTS

3.1 Neutron Diffraction. Figure 1a shows the total structure factor S(Q) (dotted line) for the CMAS-M0[32] and CMAS-M2 glass compositions derived from neutron diffraction for Q values in the range 0.45–9.5 Å⁻¹. The diffraction patterns display broad lines confirming the short and medium-range structural disorder of the materials. Apart from the variation in intensity, the spectrum recorded for the CMAS-M2 glass appears broader in the higher Q ranges than that of the CMAS-M0 glass. The calculated S(Q) (continuous line) from the RMC model was also compared with experimental S(Q), Fig. 1a, indicating excellent quantitative agreement.

In general, the position and width of the peak in the pair-correlation function $g_{ij}(r)$ reflects the value and the distribution of the distances for different atomic-pair correlations. The oxygen-linked $g_{i-O}(r)$ (where i = Ca, Mg, Al, Si and O) curves for CMAS-M0 and CMAS-M2 glasses are shown in Fig. S1. The position of the first peak maxima is associated with an interatomic distance between the oxygen anion and the cation.

Table 2: NMR parameters obtained from deconvolution of the spectra.

	CMAS-M0			CMAS-M1			CMAS-M2	
Unit	δ_{iso} (ppm)	Amount (%)	Unit	δ_{iso} (ppm)	Amount (%)	Unit	δ_{iso} (ppm)	Amount (%)
Q^0(0Al)	-66.0	0.46	Q^0(0Al)	-66.44	1.13	Q^0(0Al)	-66.36	2.19
Q^2(2Al)	-76.7	46.52	Q^1(0Al)	-76.4	62.12	Q^1(0Al)	-76.32	33.51
Q^2(0Al)	-81.4	49.68	Q^2(0Al)	-81.26	6.46	Q^2(0Al)	-82.21	22.83
Q^3(1Al)	-88.2	1.15	Q^4(3Al)	-84.83	26.07	Q^3(1Al)	-88.1	35.52
Q^4(1Al)	-97.3	2.18	Q^4(1Al)	-93.82	4.22	Q^4(0Al)	-98.51	5.95
					% Al in various units			
	(%)			(%)			(%)	
Al^{IV} (Al)		60	Al^{IV} (Al)		33	Al^{IV} (Al)		14
Al^{IV} (Si)		36	Al^{IV} (Si)		57	Al^{IV} (Si)		75
Al^{VI}		4	Al^{VI}		10	Al^{VI}		11
				Chemical composition in mol%				
RO	Al_2O_3	SiO_2	RO	Al_2O_3	SiO_2	RO	Al_2O_3	SiO_2
48.4	12.9	38.7	48.8	7.9	43.3	48.2	2.9	48.9

Table 3: Optimized parameters determined from deconvolution of the ^{29}Si MAS-NMR spectra

	$\delta(Q^4(0Al))$ (ppm)	α (ppm)	β (ppm)	R^2
CMAS-M0	100.2	8.6	3.2	2.8
CMAS-M1	97.2	7.5	4.0	4.8
CMAS-M2	98.5	7.9	5.8	4.8

Bond-length values for Si–O, Al–O, Mg–O and Ca–O pairs for both glasses are listed in Table 1. The Si–O bond length increased from 1.60 to 1.62 Å and the Ca–O bond length decreased from 2.35 to 2.30 Å on substitution of MgO for CaO and SiO2 for Al₂O₃ in the CMAS-M0 glass composition. The obtained Si–O bond length values are consistent with those expected for an ideal SiO₄ tetrahedron. The changes in Si–O and Ca–O bond lengths may be explained based on the interaction of non-network cations with the oxygen atoms. It has been clarified from a study of a series of sodium-silicate glasses that increasing the sodium content increases the Si–O bond distances by distributing the Na atoms homogeneously around oxygen species (both bridging and non-bridging).[36] Increasing sodium contents also decreased the average Na–O bond distance due to greater NBO coordination around sodium because of the shorter bond lengths of

Na–NBO compared to Na–BO.[36] The decrease in Ca–O bond length with an increase in MgO concentration reveals its preferential role as network modifier instead of charge compensator. The $g_{Mg-O}(r)$ correlation functions (Fig. S1) showed a single peak at 1.70 Å for CMAS-M0 whereas two peaks at 1.70 and 2.15 Å were observed for the CMAS-M2 glass. The appearance of $g_{Mg-O}(r)$ correlation peaks at 1.70 Å and 2.15 Å indicate the presence of

fourfold-coordinated Mg species in both CMAS-M0 and CMAS-M2 glasses and an additional six-fold coordinated Mg species in CMAS-M2 glass, respectively.[37,38] Negligible changes in bond lengths were observed for Al–O. Within experimental error, the Si–O and Al–O values agree well with the characteristic values of 1.60 Å for Si–O, and 1.75 Å for Al–O for multicomponent aluminosilicate glass.[39] The RMC simulations yielded average coordination numbers (Fig. S2) which are nearly equal to four for both Al and Si in CMAS-M0 and CMAS-M2 glass compositions, indicating concomitant four-fold coordination of both Si and Al, consistent with a silicate network formed of corner-sharing SiO₄ tetrahedra. Therefore, the initial RMC constraint is fulfilled since Si atoms are coordinated on average to 4.00 oxygen neighbours.

3.2 ^{29}Si and ^{27}Al MAS NMR for glasses. Figure 2 shows the ^{29}Si MAS NMR spectra recorded for the modified CMAS-glass series along with the deconvoluted curves. In general, coexisting tetrahedral units in aluminosilicate

glasses can be described as $Q_{Si}^n(mAl)$, where n represents the number of bridging oxygens and m represents the number of NNN Al tetrahedral units substituted for Si tetrahedra.[40–43] The n and m values (varying between 0 and 4) determine the extent of ^{29}Si MAS NMR chemical shift; changes from n→ n–1 or from m → m+1 lead to about 8–12 and 4–6 ppm increases in chemical shift, respectively.[40–44] Therefore, the chemical shift for a $Q^n(mAl)$ unit follows the additive rule and can be expressed by δ (ppm) = $-Q^4(0Al)+(4-n)\alpha+m\beta$;[13] the values for $Q^4(0Al)$, α and β are fitted against the experimental values.

The ^{29}Si MAS NMR spectrum of the CMAS-M0 glass shows a broad resonance band ranging from –60 ppm to –100 ppm with the peak maximum at –78.1 ppm. On increasing the substitution of MgO for CaO and SiO_2 for Al_2O_3, the spectra broaden and move toward lower chemical shifts with the peak maximum at –78.1 ppm for CMAS-M1 and –81.5 ppm for CMAS-M2, with the latter maintaining a shoulder at –78.1 ppm. The assymetry of the CMAS-M0 spectrum towards negative ppm, which becomes more accentuated with increasing substitution, is indicative of multiple contributions. These changes are consistent with broader distributions of bond lengths and angles, and with a more polymerised glass structure.[44] To determine the concentration of various silicate units ranging from $Q^0(mAl)$ to $Q^4(mAl)$, the ^{29}Si NMR spectra were deconvoluted with five Gaussian peaks (Fig. 2). The $Q^n(mAl)$-type units in the CMAS-M0, CMAS-M1 and CMAS-M2 glass structures were identified based on the chemical-shift values obtained from the deconvolution. The NMR parameters related to deconvolution and the fitting parameters for chemical shift values are presented in Tables 2 and 3, respectively.

The ^{27}Al MAS NMR spectrum (Fig. S3) of CMAS-M0 glass is characterised by a single broad assymetric resonance along with a tail towards negative ppm, a shape typical for glass materials, again indicating a distribution of multiple contributions. Chemical-shift values of 70.4 ppm, 67.4 ppm and 65.5 ppm (Fig. S3) were obtained on fitting the ^{27}Al MAS-NMR spectra with a single Czejeck distribution model according to Neuville et al.;[45] quadrupolar coupling constants (CQ) are 6.9, 6.3 and 6.2 MHz for CMAS-M0, CMAS-M1 and CMAS-M2, respectively. The chemical-shift values lowered with increasing substitution of Si for Al and Mg for Ca, reflecting the increasing presence of $Al_{[4]}$ units involved in Al–O–Si linkages.[13] Nevertheless, the possible formation of $Al_{[4]}$–O–$Al_{[4]}$ bonds[21,23,46] should not be excluded based on the observed chemical shifts. Chemical-composition calculations (Table 2) based on the ^{29}Si MAS NMR analysis clearly suggest the existence of $Al_{[4]}$-O-$Al_{[4]}$ units in the present glass system.

3.3 XRD of GCs. Phase analysis of XRD data for both CMAS-M1 and CMAS-M2 revealed a complex picture with at least four and two identifiable phases, respectively. Phase analysis for CMAS-M0 GCs is provided in our previous article.[32] In the case of CMAS-M1, Rietveld analysis

proceeded with refinement of melilite-based phase with nominal composition $Ca_2Mg_{0.35}Al_{1.3}Si_{1.35}O_7$ (space group, $P\bar{4}2_1m$), augite of composition $CaMg_{1-x}Al_x(Si_{1-x/2}Al_x)_2O_6$ (C2/c), $MgSiO_3$ (P2$_1$/c) and a dehydrated form of gismondine ($CaSi_2Al_2O_8$, $C\bar{1}$). For CMAS-M2, the XRD pattern revealed the presence of augite and wollastonite ($CaSiO_3$, $P\bar{1}$) as majority phases. In both cases, although vestiges of minor phase may additionally be present, these could not be identified nor refined due to the complexity of the patterns. The structural models employed in the refinements were based on results from our previous studies or earlier published structural data.[7,32,47–49] Because of the large number of refineable parameters in both refinements, thermal vibration factors, occupancies and certain atomic positions were fixed throughout the analysis. However, in the case of augite present in CMAS-M2, the large quantity of this phase made refinement of the atomic positions possible. The observed and calculated diffraction patterns, and the difference between observed and calculated diffraction patterns are shown in Fig. 1b and in Fig. S4 for CMAS-M1 GC and CMAS-M2 GC, respectively. Selected structural parameters, agreement factors and the relative amounts of crystallised fractions are listed in Tables S1 and S2 for CMAS-M1 and CMAS-M2, respectively.

3.4 ^{29}Si and ^{27}Al MAS NMR of GCs. ^{29}Si MAS NMR spectra of GCs heat treated at 850 °C for 250 h are presented in Fig. 3. The linewidth of each peak decreased considerably in comparison to that of the corresponding glasses owing to the presence of silicon in the formed crystalline phases. This higher cristallinity and rigidity is also confirmed by the drastic increase in the spin-lattice relaxation time, T1, by a factor of about 30. In general, any phase in which all Si sites are crystallographically equivalent exhibits a single ^{29}Si MAS NMR peak, whereas phases with non-equivalent Si sites originate as many peaks as there are sites. Indeed, each non-equivalent site has slightly different environments around it and therefore possesses different chemical shift.[50] These features confer a powerful complementarity of ^{29}Si MAS NMR to XRD in correlating the structure with the identified crystalline phases.

The ^{29}Si MAS NMR spectra of the GCs may be deconvoluted into several components for samples CMAS-M1 and CMAS-M2, Fig. 3. The deconvolution of the ^{29}Si MAS NMR spectra of CMAS-M0 GC may be found elsewhere.[32] The ^{29}Si MAS NMR spectrum for CMAS-M0 GC exhibits two main regions of resonances between –69 and –79 ppm and between –79 and –95 ppm, each of which is composed of several overlapping peaks. Based on their chemical shifts[50] and XRD phase analysis, these two areas are assigned to melilite-type akermanite-gehlenite ($Ca_2Mg_{1-x}Al_{2x}Si_{2-x}O_7$ where x varies from 0 to 1) and anorthite-type ($CaAl_2Si_2O_8$) crystalline phases, respectively. For synthetic gehlenite-akermanite and anorthite crystals, the respective chemical shifts were observed in the ranges of –71 - –85 ppm[44,50] and –82 - –100 ppm,[50,51] respectively. The existence of several overlapping peaks, especially for the akermanite-gehlenite region, may be easily explained

by the presence of various types of silicate tetrahedral units in a melilite-type crystalline phase surrounded by different cations, for example Al and Mg in their four-coordination forms. As in the case of CMAS-M0 GC, the ^{29}Si MAS NMR spectrum for CMAS-M1 GC exhibits overlapping peaks in a region between −69 and −79 ppm, which are assigned to akermanite-gehlenite. The overlapping peaks are sharper here than for CMAS-M0 GC indicating a higher crystallinity. The assignement of peaks for CMAS-M1 GCs was performed based on the XRD refinement results (in mol%). The second major phase according to XRD refinement is augite ($CaMg_{1-x}Al_x(Si_{1-x/2}Al_x)_2O_6$), which has an expected ^{29}Si chemical shift similar to other inosilicates like diopside (-85 ppm) or wollastonite (-86 and -9 ppm).[52,53] Therefore, the second main peak, at −84 ppm is assigned to augite.[44,50] Finally, the peak at −80.9 ppm is attributed to crystalline $MgSiO_3$,[50] and the resonances at around −95 ppm are assigned to anorthite.[32] In contrast to CMAS-M0 and CMAS-M1 GCs, the ^{29}Si MAS NMR spectrum of CMAS-M2 GC does not show any resonances belonging to akermanite-gehlenite phase, as also confirmed by XRD. In the composition CMAS-M2, the major peaks which were quantified by XRD refinement are augite and wollastonite. [52,53] As said previously, both augite and wollastonite have a chemical shift of about -85 ppm. Thus, the largest peak in the ^{29}Si NMR spectrum for the GC sample of CMAS-M2, at −84 ppm, (Fig. 3b) is attributed to augite and wollastonite. This peak corresponds to 72% of the entire Si present in the sample. In augite, when Al is substituted for Mg, Al adopts 6-fold coordination and acts as network modifier. The sharp peak close to zero ppm in the ^{27}Al NMR spectrum, (Fig. S5), is assigned to these Al^{VI} species in the augite phase. These Al-substituted species may also give rise to additional ^{29}Si peaks at slightly higher and/or lower chemical shift those of augite. Indeed, similar effects have previously been observed for diopside.[52,53] However, the presence of other phases and/or glass (not seen in XRD) may also explain some of the small ^{29}Si peaks.

The ^{27}Al NMR spectra for the GCs were deconvoluted using peaks based on the Czejeck distribution model and a peak with second-order quadrupolar effects (Fig. S5, Table S3). The ^{27}Al MAS NMR spectrum of CMAS-M0 GC shows a single resonance peak at about 68 ppm (highest point at 60.8 ppm), indicating that most Al exists in four-fold coordination. The slight shoulder at 80 ppm may be attributable to a minor phase present in the sample. As expected, the peak width decreased considerably in comparison to the corresponding CMAS-M0 glass spectrum, confirming the higher order and, therefore, higher crystallinity in this sample. This suggests that the majority of AlO_4 units exist in crystalline phases, most likely in anorthite where $Al_{[4]}$ units are preferentialy formed, as well as in melilite-type akermanite-gehlenite. On the other hand, the ^{27}Al MAS NMR spectra of CMAS-M1 and CMAS-M2 GC spectra both exhibit a main peak at 68 ppm characteristic of $Al_{[4]}$, as in the case for CMAS-M0 GC, and a second peak at about 0 − 5, typical of a $Al_{[6]}$ environment, likely existing in diopside phase. The relative intensity of the $Al_{[6]}$ peak compared to that of $Al_{[4]}$ is much higher in CMAS-M2 GC (32 % of $Al_{[6]}$ vs 68 % of $Al_{[4]}$) than in CMAS-M1 GC (10 % of $Al_{[6]}$ vs 90 % of $Al_{[4]}$), in good agreement with the higher fraction of diopside formed in CMAS-M2 GC. Additionally, the enhanced sharpness of this $Al_{[6]}$ peak is a clear indication that most AlO_6 units exist in crystalline phase. Accordingly, deconvolution analysis revealed the fraction of 4-coordinated Al in CMAS-M1 and CMAS-M2 as ~80 and ~67%, respectively. In CMAS-M0, however, the entire Al content remains in the 4-coordinated state.[32] The details of the deconvolution are presented in Table S3. The peak appearing at 80 ppm in the CMAS-M0 GC spectrum has no analogous contributions in the CMAS-M1 and CMAS-M2 spectra (Fig. S5), indicating that it is solely due to the presence of anorthite. According to single-crystal NMR analysis,[54] anorthite contains eight $Al_{[4]}$ sites and the small peak at 80 ppm can be assigned to a low fraction of Al tetrahedra through the formation of Al−O−Al linkages.[13,55]

3.5 Raman studies. Structural changes with increasing temperature were assessed by the Raman spectra collected for GC samples heat treated at 100 °C and 800 °C, Fig. 4. Complete spectra for all the glasses during the heat treatment from 100 °C to 800 °C are presented in Fig. S6. Broadly speaking, the Raman spectra can be divided into three frequency regions: (i) 800–1200 cm^{-1}, due to symmetric stretching motions of terminal non-bridging oxygens of SiO_4, denoted as the $v_s(Si–O-)$ region; (ii) 500–800 cm^{-1}, accounting for asymmetric stretching vibrations of bridging oxygens situated between two tetrahedra, denoted as the $v_s(T–O–T)$ region, where T=Al or Si; (iii) 200–500 cm^{-1}, representative of non-network cation vibrations, also called lattice vibations involving modifier cations, in the present case Ca^{2+} and Mg^{2+}.

The four broad Raman vibrational bands in the CMAS-M0 spectra (Fig. 4) at 926 cm^{-1}, 662 cm^{-1} and at 323 cm^{-1} can be assigned to $v_s(Si–O^-)$ and $v_s(T–O–T)$, where T=Al or Si, and lattice vibrations of structural units present in melilite-type akermanite-gehlenite phases, respectively. The bands at 430 cm^{-1} and 530 cm^{-1} are attributable to $v_s(Si–O–Si)$, and $v_s(Si–O–Al)$ vibrations present in anorthite, respectively.[32] On increasing the heat-treatment temperature from 100 to 800 °C, the intensity of the high-frequency Raman band at 800–1200 cm^{-1} decreased more relative to that of lower frequency bands. This is attributed to distortions of the SiO_4 tetrahedra. In addition, the intensity of the band appearing at 430 cm^{-1} decreased and merged with the band appearing at 530 cm^{-1}.

The Raman spectra of CMAS-M1, Fig. 4, are similar to those of CMAS-M0 except for slight shifts in peak positions to lower resonance frequencies, and the presence of two additional resonance peaks at 1018 cm^{-1} in region I and at 406 cm^{-1} in region III. Based on the XRD phase analysis, the Raman resonance frequencies in CMAS-M1 may be assigned as follows:[11,56] the bands at 1018 cm^{-1} and 922 cm^{-1} correspond to $v_s(Si–O^-)$ vibrations of diopside and melilite-type akermanite-gehlenite phases, respectively; the band at 669 cm^{-1} corresponds to $v_s(Si–O–T)$ mode vibrations of both diopside and melilite-type akermanite-gehlenite phases; the bands at 406 and 326 cm^{-1}

correspond to non-tetrahedral cation–oxygen stretching bonds (lattice vibrational modes). With increasing temperature, the bands in the higher frequency region at 1018, 922 and 669 cm^{-1} tend to shift slightly towards lower frequency. For other bands, except small variations in intensities, no other significant changes in peak positions are observed with increase in temperature up to 800 °C.

The Raman spectra of CMAS-M2, (Fig. 4), display four strong resonance bands at 1018, 667, 402 and at 347 cm^{-1}, which all slightly shift towards lower frequencies upon increasing the heat-treatment temperature. This shift suggests that all the cation–oxygen bonds undergo some distortion as a result of heat treatment at 850 °C, whereas, in CMAS-M1, only network-former cations exhibit noticeable distortions; no influence of heat treatment has been observed in the case of CMAS-M0 GC. The spectra resemble those of synthetic diopside crystals[56] with characteristic frequencies at around 1018, 667, and (402, 347) cm^{-1}, which can be assigned to ν_s(Si–O$^-$), ν_s(Si–O–Si) and lattice vibrations, respectively. In comparison to CMAS-M0 and CMAS-M1, CMAS-M2 yielded well resolved latice vibrational modes, most probably due to greater covalent character of the bonds between modifier cations and oxygen anions.

4. DISCUSSION

The analysis of chemical composition based on the ^{29}Si NMR deconvolution results (Fig. 2 and Table 2) indicate the presence of four coordinated Al–O–Al linkages in the network structure of glasses investigated in this study. According to Loewenstein's rule,[21] Al–O–Si bonds are preferred energetically over Al–O–Al and Si–O–Si bonds in silicate melts. However, when the amount of Al$_2$O$_3$ is larger than the available –O–Si bonds, this rule must be broken or a different structure is established. In light of this, we have derived a parameter called the Aluminium Avoidance Parameter (*AAP*) to predict when there are an insufficient number of –O–Si bonds, given by equation (1):

$$AAP = \frac{4[Al_2O_3]}{2[SiO_2] - [RO] + [Al_2O_3]} \qquad (1)$$

When *AAP* ≤ 1, there are a sufficient number of –O–Si bonds available to satisfy Loewenstein's rule, whereas when *AAP* > 1, there are not. The derivation of Eq. (1) is presented in SI. In the current glass compositions, AAP values are 1.2, 0.7 and 0.2 for CMAS-M0, CMAS-M1 and CMAS-M2, respectively. Accordingly, the glass CMAS-M0 does not have a sufficient number of –O–Si bonds to satisfy Loewenstein's rule, and a different mechanism should be employed. In this case, the remaining Al$_2$O$_3$ breaks the rule and creates Al$_{[4]}$–O–Al$_{[4]}$ linkages of Al$_2$O$_3$ tetrahedra in a separate Al-rich phase. The behaviour of Al–O– is better understood on analysis of the ^{27}Al MAS NMR spectra. In aluminate glasses containing Al tetrahedra, the ^{27}Al NMR spectra exhibit chemical shifts of ~>70 ppm;[57] whereas in aluminosilicate glasses, they are ~60 ppm.[58] The presence of Al$_{[4]}$–O–Al$_{[4]}$ bonds therefore results in higher chemical-shift values. From the ^{27}Al NMR spectra (Fig. S3) of the glasses, the amount of Al in

Al$_{[4]}$–O–Al$_{[4]}$ bonds could not be determined quantitatively because of a broad peaks ranging from -40 to 100 ppm due to the second order quadrupolar broadening. Although a definable peak was not observed in the CMAS-M0 glass, the presence of Al$_{[4]}$–O–Al$_{[4]}$ bonds is confirmed from the peak observed at 80 ppm in quantitative analysis of ^{27}Al NMR spectrum of CMAS-M0 GC. However, the chemical composition calculations from ^{29}Si MAS NMR analysis indicate that 60% of Al is present as Al$_{[4]}$–O–Al$_{[4]}$ linkages. On the other hand, the *AAP* values for CMAS-M1 and CMAS-M2 point to the absence of Al$_{[4]}$–O–Al$_{[4]}$ bonds, owing to the sufficient number of available –O–Si bonds. This is not in agreement with the ^{29}Si MAS NMR analysis, which indicates the presence of 33 mol% and 14 mol% of Al in Al$_{[4]}$–O–Al$_{[4]}$ linkages, in CMAS-M1 and CMAS-M2 glasses, respectively. In addition, the fraction of Al in Al$_{[4]}$–O–Al$_{[4]}$ linkages in CMAS-M0 (60 %) is also higher than that predicted from the *AAP* analysis. This suggests that an alternative approach is required to explain the distribution of structural units and the presence of the observed crystalline phases in the glass-ceramics.

For alumina-containing silicate glasses, the MRN model was slightly modified and the following assumptions were considered by Moesgaard et al.[13] Owing to the high preference of silicon tetrahedra to bond with alumina tetrahedra, Si–O–Al bonds are preferred over Al–O–Al and Si–O–Si bonds and the overall concentration and clusters of Si–O–Al bonds is greater. If partition of the network and non-network region is accepted in the glass structure, the network-region can be further described as being composed of two regions, one consisting of SiO$_4$ and AlO$_4$ units connected through Si–O–Al bonds and the other of pure SiO$_4$ units connected through Si–O–Si units. Considering the absence of NBOs associated with the AlO$_4$ tetrahedra, the presence of alternative SiO$_4$–AlO$_4$ units in a Si/Al ratio of 1:1 results in a highly polymerized Al-containing region which follows the Al-avoidance principle. This indicates that the concentration of Al–O–Al bonds depends on the concentration of various Q^n(mAl) units present in the glass structure. The probability that the Al avoidance principle breaks down increases when Al is assigned to Si associated with a lesser number of bridging oxygens.

In the present glass system, the concentration of available modifer cations (35.5 mol% in CMAS-M0), calculated taking into account the requirement of charge compensation for Si–O–Al and Al–O–Al units in a Al/Ca ratio of 1:1, is enough to create a high concentration of non-bridging oxygens, thereby also affecting the concentration of Al–O–Al bonds, besides the Si/Al ratio. This indicates that the high concentration of Al in Al–O–Al linkages observed in the CMAS-M0 glasses results from clustering of AlO4 and SiO4 units, which are connected in the form of Q^2(2Al) assemblies in the Al/Si-network region, whilst another network region is composed of pure SiO$_4$ units connected in the form of Q^2 units. A schematic presentation of possible structural distributions in the CMAS-M0 glass is presented in Fig. 5 (left), which can be considered representative of the "new modified random network

model". The inter-network region consists of both MgO and CaO in the form of network modifiers connected to NBOs of both $Q^2(2Al)$ and Q^2 units.

It has been further observed that the percentage of Al in the Al–O–Al linkages decreases whilst the concentration of AlO_6 increases with greater substitution of Si for Al. This observation supports the hypothesis of the formation of individual and well-separated clustered regions of SiO_4/AlO_4 (Si/Al) and SiO_4 in aluminosilicate glasses. In general, the Al-coordination number increases with increasing cation-field strength in aluminosilicate glasses.[59] Although there are a sufficient number of non-network cations, especially Ca^{2+}, present in the glass system, the increasing concentration of Mg over Ca favours the role of the former as charge compensator, preferentially entering in the Al/Si region instead of Ca^{2+} cations. The small size of Mg^{2+} also favours its localization in network tetrahedral cavities, thereby competing with aluminium for network-forming positions. This reduces the role of Mg^{2+} as a charge compensator for Al in tetrahedral positions as compared to Ca^{2+}, which may result in the formation of highly-coordinated Al, and lower glass viscosity.[60] In addition, the increase in intensity of the Raman band around 400 cm^{-1} with greater substitution of Mg for Ca also clearly suggests a change in Mg coordination from tetrahedral to octahedral. In general, the observation of a vibrational band in the low-frequency region may be assigned to the presence of a modifier cation in octahedral coordination. The increase in Si–O bond length from CMAS-M0 to CMAS-M2 may also be explained based on the formation of both Al/Si- and Si-clustered regions in the glass structure (a schematic presentation of possible structural distribution in CMAS-M2 glass, along with CMAS-M1, is also presented in Fig. 5). In general, Si–O bond lengths in Si–O–Al linkages are shorter than those of average Si–O bond lengths in Si–O–Si linkages, such that greater substitution of Si for Al results in a gradual conversion of Si–O–Al into Si–O–Si bonds, increasing the overall Si–O bond length.

The above analysis can also be confirmed on consideration of the crystalline phases developed in the aluminosilicate glasses. In general, crystallization of a phase can occur when there is an adequately abundant supply of appropriate elements in the glass in the ratio demanded by the phase stoichiometry. The presence of clustered SiO_4 and $1/2CaAlO_4$ units in the Si/Al network region, and a high concentration of MgO_4 tetrahedral units in the non-network region, which are all characteristic structural units of melilite crystals,[7] led to the formation of melilite-based gehlinite-akermanite phase upon heat treating at 850 °C for 250 h. It has also been reported that the gehlenite crystal structure consist Al–O–Al linkages and a full Al/Si ordering of gehlenite is not experimentally achievable.[40] This suggests that CMAS-M0 glass contain Al–O–Al bonds. These are the responsible for the formation of gehlenite contain melilite phase in CMAS-M0 GC. The formation of melilite also suggests that the Al/Si clustered regions behave as nucleating agents and promote crystallization in comparison to the Si-clustered

region. Nevertheless, the appearance of a broad peak in the ^{29}Si MAS NMR spectrum of CMAS-M0 GCs indicates that only a limited fraction of glass was converted into melilite-type crystals, with the remaining glass phase in the Si/Al region remaining in a more polymerized condition with greater Si/Al ratio. It is to be noted at this point that with increasing the temperature or holding the temperature for longer period of time the structural rearrangement occurs as is reported in our previous report.[32] This may leads to the formation of large extent Al/Si order in remaining glassy phase after the formation of melilite phase. The enhanced Al/Si order increases the probability for the formation of anorthite crystalline phase, which generally consist large extent of Al/Si order.[32] It has been reported that the time for anorthite nucleation and growth from its own melts at 900 °C and 1050 °C takes 92 h and 48 h, respectively.[61] Structural changes observed from in-situ Raman spectra for CMAS-M0 glass (Fig. 4) clearly indicate favoured interactions among Si–O–Si (430 cm^{-1}), Si–O–Al (480 cm^{-1}) and Al–O–Al (560 cm^{-1})[62] units with increasing temperature. The formation of anorthite in CMAS-M0 GC strongly suggests that, after the formation of melilite crystals, clusters of highly polymerized alternating SiO_4 and $(1/2Ca)AlO_4$ tetrahedra in the Si/Al NS-region interact with the Si–O–Si units present in the Si-clustered NS-region through the C-region. This phenomenon generally increases the Al/Si order and likely reduces the energy barrier towards the formation of anorthite. This is in accordance with the results observed in our previous study.[32] It was found that the formation of melilite phase was completely suppressed and a major fraction of Al-containing diopside (augite), in which Al exhibits AlO_6 coordination, was formed on substitution of MgO for CaO and SiO_2 for Al_2O_3. The presence of Raman bands around 400 cm^{-1} indicated that the coordination of the Mg^{2+} cation changed from tetrahedral to octahedral. Again, one can expect that melilite and augite crystalline phases are formed from the Si/Al region. The formation of alumina-containing crystalline phases from aluminosilicate glasses indicate that the Al/Si clustered regions are more distorted than the Si clustered ones, and thereby behave as nucleating agents. On the other hand, the formation of $MgSiO_3$ in CMAS-M1 GC can be understood based on the interaction of tetrahedrally coordinated Mg^{2+} cations located in the non-network region and Si-O-Si units residing in the Si clustered region. On the other hand, $CaSiO_3$ crystallised instead of $MgSiO_3$ in CMAS-M2 GCs. This again confirms that, with increasing the degree of MgO substitution for CaO, Mg^{2+} competes with Ca^{2+} for charge compensating within the Al/Si network, favouring occupation of the non-network region with Ca^{2+}.

The changes in frequencies of Raman modes observed with increasing temperature can be clearly assigned to the longer T–O bond lengths (~1.64 Å) in diopside crystals in comparison to the T–O bond lengths in melilite (~1.619 Å) crystals.[7] However, the spectra of the CMAS-M0 glass at high temperature are more stable, indicating its higher thermal stability against devitrification in comparison to the CMAS-M1 and CMAS-M2 glasses, a favourable feature

for certain technical applications. The expected chemical shift (ECS) values (Fig. S7) of ^{29}Si over the entire spectrum also indicate the overall variation in the structure before and after crystallization. This is affected by changes both in the bond lengths and angles and in the next nearest neighbour environment of the Si atoms. The ECS value of the GCs moves to the right from CMAS-M0 to CMAS-M2, showing an increased shielding effect in comparison to the corresponding glass samples. In-situ XRD results (Fig. S8) also revealed decreased thermal stability going from composition CMAS-M0 to CMAS-M2, probably because of the high concentration of non-network cations.

5. CONCLUSIONS

The structure and crystallization behaviour of modified CMAS glasses with important technological applications has been revealed from experimental data gathered through a number of complementary advanced characterisation techniques (ND, XRD, MAS NMR and *in-situ* Raman). Preventing the Al-Avoidance principle within the framework of a modified random-network model explains the distribution of structural units in the network structure of aluminosilicate glasses. The glass structure consists of a network-structure region (NS-Region) composed of framework species, that can be further described as two NS-regions containing SiO_4 and AlO_4 (Si/Al) units, referred to here as a new modified random network (NMRN) model. Simulations of chemical composition based on deconvolution of ^{29}Si MAS-NMR spectra support the concept of circumventing the Al-avoidance principle in aluminosilicate glasses. $Al_{[4]}$–O–$Al_{[4]}$ bonds are highly favoured in the presence of a high concentration of NBOs and insufficient –O–Si bonds in the Si/Al NS-region. It is also concluded that the field strength of the charge-compensator cation influences the coordination of Al^{3+} in the Si/Al-containing NS-region. The crystalline phases formed upon heat treating the glasses at 850 °C for 250 h may be considered to account for the distribution of SiO_4 and AlO_4 structural units. The as-formed Al/Si-NS regions in aluminosilicate glasses behave as nucleating agents, favouring crystallization in comparison to the Si-clustered region. In addition, the interaction between the Si/Al NS-region and SiO_4-rich NS-region through the C-region at higher temperatures results in the formation of secondary crystalline phases.

ASSOCIATED CONTENT

Supporting Information.
 Supporting Information is available free of charge at http://pubs.acs.org.

Detailed experimental procedure, ^{27}Al MAS NMR and deconvolution results, *in-situ* Raman spectra, *in-situ* XRD spectra, X-ray Photoelectron Spectroscopy analysis and the schematic picture representing the formation of cluster and channel region obtained from Molecular dynamics simulations for CMAS-M0 glass.

AUTHOR INFORMATION

Corresponding Author

*E-mail: aareddy@cgcri.res.in (A.R.A.).
*E-mail: jmf@ua.pt (J.M.F.F.).
Phone.: +351-234-370242. Fax: +351-234-370204

Author Contributions

ACKNOWLEDGMENT

REFERENCES

(1)   Lee, S. K.; Kim, H.-I.; Kim, E. J.; Mun, K. Y.; Ryu, S. Extent of Disorder in Magnesium Aluminosilicate Glasses: Insights from 27Al and 17O NMR. *J. Phys. Chem. C* **2016**, *120* (1), 737–749.
(2)   Ross, S.; Welsch, A.-M.; Behrens, H. Lithium Conductivity in Glasses of the Li2O-Al2O3-SiO2 System. *Phys. Chem. Chem. Phys.* **2014**, *17* (1), 465–474.
(3)   Calahoo, C.; Zwanziger, J. W.; Butler, I. S. Mechanical–structural Investigation of Ion-Exchanged Lithium Silicate Glass Using Micro-Raman Spectroscopy. *J. Phys. Chem. C* **2016**, *120* (13), 7213–7232.
(4)   Tiegel, M.; Herrmann, A.; Russel, C.; Korner, J.; Klopfel, D.; Hein, J.; Kaluza, M. C. Magnesium Aluminosilicate Glasses as Potential Laser Host Material for Ultrahigh Power Laser Systems. *J. Mater. Chem. C* **2013**, *1* (33), 5031–5039.
(5)   Bischoff, C.; Eckert, H.; Apel, E.; Rheinberger, V. M.; Holand, W. Phase Evolution in Lithium Disilicate Glass-Ceramics Based on Non-Stoichiometric Compositions of a Multi-Component System: Structural Studies by 29Si Single and Double

Resonance Solid State NMR. *Phys. Chem. Chem. Phys.* **2011**, *13* (10), 4540–4551.

(6) Malavasi, G.; Pedone, A.; Menziani, M. C. Study of the Structural Role of Gallium and Aluminum in 45S5 Bioactive Glasses by Molecular Dynamics Simulations. *J. Phys. Chem. B* **2013**, *117* (15), 4142–4150.

(7) Reddy, A. A.; Tulyaganov, D. U.; Mather, G. C.; Rodríguez-López, S.; Das, S.; Pascual, M. J.; Muñoz, F.; Siegel, R.; Senker, J.; Ferreira, J. M. F. Influence of Strontium Oxide on Structural Transformations in Diopside-Based Glass-Ceramics Assessed by Diverse Structural Tools. *J. Phys. Chem. C* **2015**, *119* (21), 11482–11492.

(8) Goel, A.; Reddy, A. A.; Pascual, M. J.; Gremillard, L.; Malchere, A.; Ferreira, J. M. F. Sintering Behavior of Lanthanide-Containing Glass-Ceramic Sealants for Solid Oxide Fuel Cells. *J. Mater. Chem.* **2012**, *22* (19), 10042–10054.

(9) Thieme, C.; Waurischk, T.; Heitmann, S.; Rüssel, C. New Family of Materials with Negative Coefficients of Thermal Expansion: The Effect of MgO, CoO, MnO, NiO, or CuO on the Phase Stability and Thermal Expansion of Solid Solution Phases Derived from $BaZn_2Si_2O_7$. *Inorg. Chem.* **2016**, *55* (9), 4476–4484.

(10) Eden, M. NMR Studies of Oxide-Based Glasses. *Annu. Reports Sect. "C" (Physical Chem.* **2012**, *108* (1), 177–221.

(11) Sharma, S. K.; Yoder, H. S.; Matson, D. W. Raman Study of Some Melilites in Crystalline and Glassy States. *Geochim. Cosmochim. Acta* **1988**, *52* (8), 1961–1967.

(12) Sváb, M. F. and T. P. and U. R. and E. V. and E. Uranium Surroundings in Borosilicate Glass from Neutron and X-Ray Diffraction and RMC Modelling. *J. Phys. Condens. Matter* **2010**, *22* (40), 404206.

(13) Moesgaard, M.; Keding, R.; Skibsted, J.; Yue, Y. Evidence of Intermediate-Range Order Heterogeneity in Calcium Aluminosilicate Glasses. *Chem. Mater.* **2010**, *22* (15), 4471–4483.

(14) Farnan, I.; Stebbins, J. F. High-Temperature Silicon-29 NMR Investigation of Solid and Molten Silicates. *J. Am. Chem. Soc.* **1990**, *112* (1), 32–39.

(15) Hehlen, B.; Neuville, D. R. Raman Response of Network Modifier Cations in Alumino-Silicate Glasses. *J. Phys. Chem. B* **2015**, *119* (10), 4093–4098.

(16) McCarty, R. J.; Stebbins, J. F. Transition Metal Dopant Cation Distributions in MgO and CaO: New Inferences from Paramagnetically Shifted Resonances in ^{17}O, [25]Mg, and [43]Ca NMR Spectra. *J. Phys. Chem. C* **2016**, *120* (20), 11111–11120.

(17) Zheng, Q.; Potuzak, M.; Mauro, J. C.; Smedskjaer, M. M.; Youngman, R. E.; Yue, Y. Composition–structure–property Relationships in Boroaluminosilicate Glasses. *J. Non. Cryst. Solids* **2012**, *358* (6), 993–1002.

(18) Lee, S. K.; Cody, G. D.; Mysen, B. O. Structure and the Extent of Disorder in Quaternary (Ca-Mg and Ca-Na) Aluminosilicate Glasses and Melts. *American Mineralogist*. 2005, pp 1393–1401.

(19) Lee, S. K. Microscopic Origins of Macroscopic Properties of Silicate Melts and Glasses at Ambient and High Pressure: Implications for Melt Generation and Dynamics. *Geochim. Cosmochim. Acta* **2005**, *69* (14), 3695–3710.

(20) Smedskjaer, M. M.; Mauro, J. C.; Kjeldsen, J.; Yue, Y. Microscopic Origins of Compositional Trends in Aluminosilicate Glass Properties. *J. Am. Ceram. Soc.* **2013**, *96* (5), 1436–1443.

(21) Loewenstein, W. The Distribution of Aluminum in the Tetrahedra of Silicates and Aluminates. *Am. Mineral.* **1954**, *39*, 92–96.

(22) Greaves, G. N. EXAFS and the Structure of Glass. *J. Non. Cryst. Solids* **1985**, *71* (1), 203–217.

(23) Stebbins, J. Aluminium Avoidance Avoided. *Nature* **1987**, *330* (6143), 13–14.

(24) Lee, S. K.; Stebbins, J. F. The Structure of Aluminosilicate Glasses: High-Resolution ^{17}O and ^{27}Al MAS and 3QMAS NMR Study. *J. Phys. Chem. B* **2000**, *104* (17), 4091–4100.

(25) Stebbins, J.; Zhao, P.; Cheng, X. Reactive Al-O-Al Sites in a Natural Zeolite: Triple-Quantum Oxygen-17 Nuclear Magnetic Resonance. *Am. Mineral.* **1999**, *84*, 1680–1684.

(26) Fletcher, R. E.; Ling, S.; Slater, B. Violations of Lowenstein's Rule in Zeolites. *Chem. Sci.* **2017**, *8* (11), 7483–7491.

(27) Lee, S.; Stebbins, J. The Degree of Aluminum Avoidance in Aluminum Silicate Glasses. *Am. Mineral.* **1999**, *84*, 937–945.

(28) de Jong, B. H. W. S.; Brown, G. E. Polymerization of Silicate and Aluminate Tetrahedra in Glasses, Melts and Aqueous solutions—II. The Network Modifying Effects of Mg2+, K+, Na+, Li+, H+, OH–, F–, Cl–, H_2O, CO_2 and H_3O+ on Silicate Polymers. *Geochim. Cosmochim. Acta* **1980**, *44* (11), 1627–1642.

(29) Lee, S. K.; Kim, H.; Kim, E. J.; Mun, K. Y.; Ryu, S. Extent of Disorder in Magnesium Aluminosilicate Glasses: Insights from 27 Al and 17 O NMR. **2016**.

(30) Sukenaga, S.; Florian, P.; Kanehashi, K.; Shibata, H.; Saito, N.; Nakashima, K.; Massiot, D. Oxygen Speciation in Multicomponent Silicate Glasses Using through Bond Double Resonance NMR Spectroscopy. *J. Phys. Chem. Lett.* **2017**, *8* (10), 2274–2279.

(31) Magi, M.; Lippmaa, E.; Samoson, a.; Engelhardt, G.; Grimmer, a. R. Solid-State High-Resolution Silicon-29 Chemical Shifts in Silicates. *J. Phys. Chem.* **1984**, *88* (8), 1518–1522.

(32) Allu, A. R.; Balaji, S.; Tulyaganov, D. U.; Mather, G. C.; Margit, F.; Pascual, M. J.; Siegel, R.; Milius, W.; Senker, J.; Agarkov, D. A.; et al. Understanding the Formation of $CaAl_2Si_2O_8$ in

Melilite-Based Glass-Ceramics: Combined Diffraction and Spectroscopic Studies. *ACS Omega* **2017**, 2 (9), 6233–6243.

(33)   Amarnath, A.; Goel, A.; Tulyaganov, D. U.; Kapoor, S.; Pradeesh, K.; Pascual, M. J.; Ferreira, J. M. F. Study of Calcium E Magnesium E Aluminum E Silicate (CMAS) Glass and Glass-Ceramic Sealant for Solid Oxide Fuel Cells. *J. Power Sources* **2013**, 231, 203–212.

(34)   Sváb, E.; Mészáros, G.; Deák, F. Neutron Powder Diffractometer at the Budapest Research Reactor. *Mater. Sci. Forum* **1996**, 228–231, 247–252.

(35)   Rodríguez-Carvajal, J. Recent Advances in Magnetic Structure Determination by Neutron Powder Diffraction. *Phys. B Condens. Matter* **1993**, 192 (1), 55–69.

(36)   Angeli, F.; Villain, O.; Schuller, S.; Ispas, S.; Charpentier, T. Insight into Sodium Silicate Glass Structural Organization by Multinuclear NMR Combined with First-Principles Calculations. *Geochim. Cosmochim. Acta* **2011**, 75 (9), 2453–2469.

(37)   Krezhov, M. F. and E. S. and K. Network Structure of Molybdate Glasses by Neutron and X-Ray Diffraction and Reverse Monte Carlo Modelling. *J. Phys. Conf. Ser.* **2016**, 746 (1), 12068.

(38)   Fiske, P. S.; Stebbins, J. F. The Structural Role of Mg in Silicate Liquids: A High-Temperature 25Mg, 23Na, and 29Si NMR Study. *Am. Mineral.* **1994**, 79 (9–10), 848–861.

(39)   Guignard, M.; Cormier, L. Environments of Mg and Al in MgO-Al2O3-SiO2 Glasses: A Study Coupling Neutron and X-Ray Diffraction and Reverse Monte Carlo Modeling. *Chem. Geol.* **2008**, 256 (3–4), 110–117.

(40)   Florian, P.; Veron, E.; Green, T. F. G.; Yates, J. R.; Massiot, D. Elucidation of the Al/Si Ordering in Gehlenite Ca2Al2SiO7 by Combined 29Si and 27Al NMR Spectroscopy/Quantum Chemical Calculations. *Chem. Mater.* **2012**, 24 (21), 4068–4079.

(41)   Florian, P.; Fayon, F.; Massiot, D. 2J Si–O–Si Scalar Spin–Spin Coupling in the Solid State: Crystalline and Glassy Wollastonite CaSiO3. *J. Phys. Chem. C* **2009**, 113 (6), 2562–2572.

(42)   Iftekhar, S.; Pahari, B.; Okhotnikov, K.; Jaworski, A.; Stevensson, B.; Grins, J.; Edén, M. Properties and Structures of RE2O3–Al2O3–SiO2 (RE = Y, Lu) Glasses Probed by Molecular Dynamics Simulations and Solid-State NMR: The Roles of Aluminum and Rare-Earth Ions for Dictating the Microhardness. *J. Phys. Chem. C* **2012**, 116 (34), 18394–18406.

(43)   Murdoch, J. B.; Stebbins, J. F.; Carmichael, I. S. E.; Pines, A. A Silicon-29 Nuclear Magnetic Resonance Study of Silicon-Aluminum Ordering in Leucite and Analcite. *Phys. Chem. Miner.* **1988**, 15 (4), 370–382.

(44)   Murdoch, J. B.; Stebbins, J. F. High-Resolution 29Si NMR Study of Silicate and Aluminosilicate Glasses: The Effect of Network-Modifying Cations. *Am.*

Mineral. **1985**, 70, 332–343.

(45)   Neuville, D. R.; Cormier, L.; Massiot, D. Al Environment in Tectosilicate and Peraluminous Glasses: A 27Al MQ-MAS NMR, Raman, and XANES Investigation. *Geochim. Cosmochim. Acta* **2004**, 68 (24), 5071–5079.

(46)   The Degree of Aluminum Avoidance in Aluminosilicate Glasses . *American Mineralogist* . 1999, p 937.

(47)   Buerger, M. J.; Prewitt, C. T. The Crystal Structures of Wollastonite and Pectolite. *Proc. Natl. Acad. Sci. U. S. A.* **1961**, 47 (12), 1884–1888.

(48)   The Crystal Structures of Clinoenstatite and Pigeonite . *Zeitschrift für Kristallographie - Crystalline Materials* . 1960, p 120.

(49)   Topotactic Transformation and Dehydration of the Zeolite Gismondine to a Novel Ca Feldspar Structure . *American Mineralogist* . 2013, p 1988.

(50)   Smith, K. A.; Kirkpatrick, R. J.; Oldfield, E.; Henderson, D. M. High-Resolution Silicon-29 Nuclear Magnetic Resonance Spectroscopic Study of Rock-Forming Silicates. *Am. Mineral.* **1983**, 68 (11–12), 1206–1215.

(51)   Phillips, B. L.; Kirkpatrick, R. J.; Carpenter, M. A. Investigation of Short-Range Al,Si Order in Synthetic Anorthite by 29Si MAS NMR Spectroscopy. *Am. Mineral.* **1992**, 77 (5–6), 484–494.

(52)   Hayashi, S.; Okada, K.; Otsuka, N. Characterization of MgSiO3, CaMgSi2O6 and CaSiO3 Precursor Powders by 29Si MAS NMR. *J. Eur. Ceram. Soc.* **1994**, 14 (1), 61–66.

(53)   Flemming, R. L.; Luth, R. W. 29Si MAS NMR Study of diopside–Ca-Tschermak Clinopyroxenes: Detecting Both Tetrahedral and Octahedral Al Substitution. *Am. Mineral.* **2002**, 87, 25–36.

(54)   Brinkmann, D.; Staehli, J. L. Magnetische Kernresonanz von 27Al Im Anorthit, CaAl2Si2O8. *Helv. Phys. Acta* **1968**, 41, 274–281.

(55)   Larsen, F. H.; Farnan, I. Site Populations and Short Range Order in Aluminosilicates Investigated by 27Al Solid-State NMR. *J. Phys. Chem. B* **2004**, 108 (28), 9764–9771.
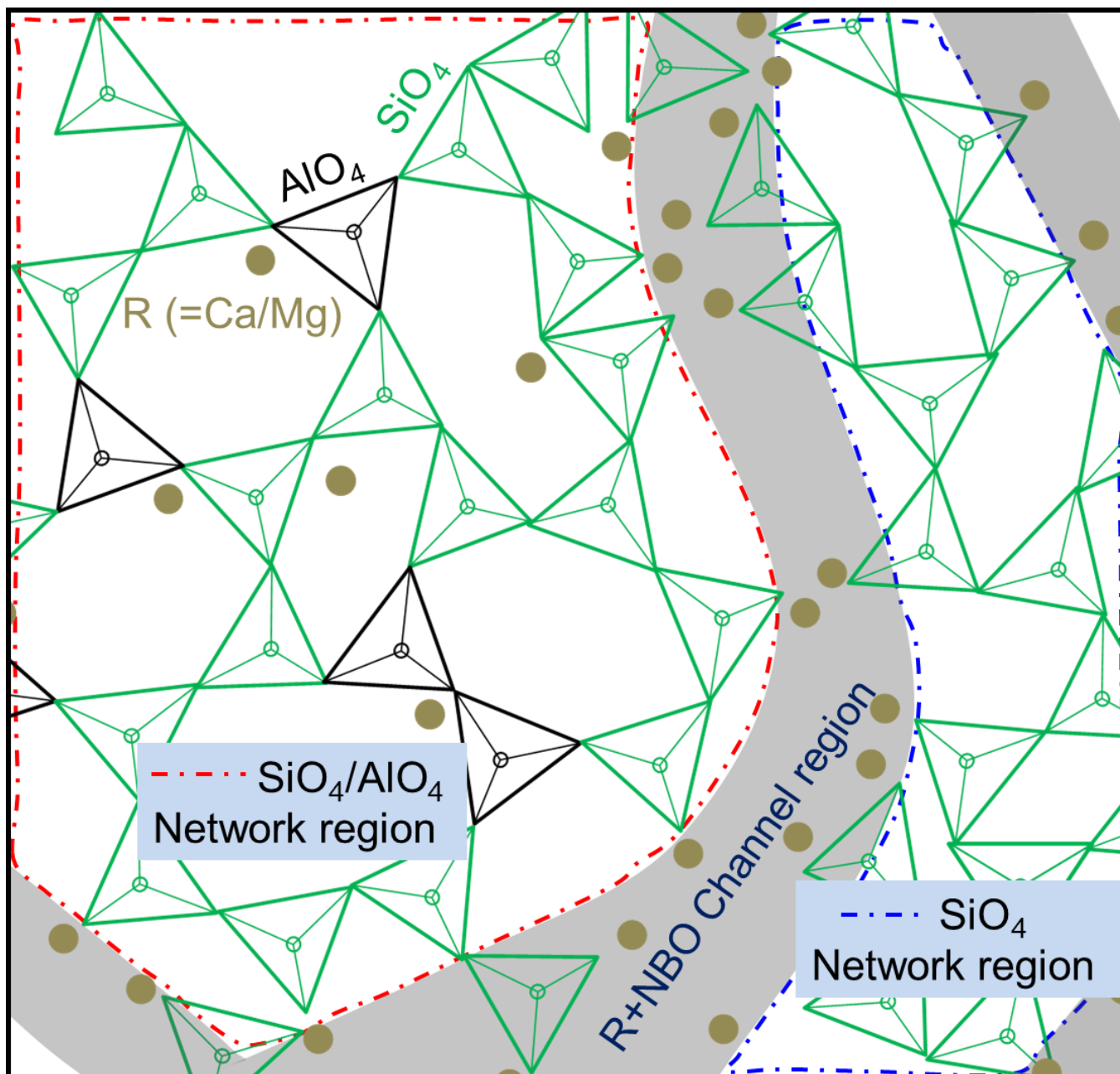
(56)   Richet, P.; Mysen, B. O.; Ingrin, J. High-Temperature X-Ray Diffraction and Raman Spectroscopy of Diopside and Pseudowollastonite. *Phys. Chem. Miner.* **1998**, 25 (6), 401–414.

(57)   Licheron, M.; Montouillout, V.; Millot, F.; Neuville, D. R. Raman and 27 Al NMR Structure Investigations of Aluminate Glasses : (1 – X) Al 2 O 3 – X MO , with M = Ca , Sr , Ba and 0 . 5 B X B 0 . 75). *J. Non. Cryst. Solids* **2011**, 357 (15), 2796–2801.

(58)   Quintas, A.; Caurant, D.; Majérus, O.; Charpentier, T.; Dussossoy, J.-L. Effect of Compositional Variations on Charge Compensation of AlO4 and BO4 Entities and on Crystallization Tendency of a Rare-Earth-Rich Aluminoborosilicate Glass. *Mater. Res. Bull.* **2009**, 44 (9), 1895–1898.

(59)   Florian, P.; Sadiki, N.; Massiot, D.; Coutures, J. P. 27Al NMR Study of the Structure of Lanthanum- and Yttrium-Based Aluminosilicate Glasses and Melts. *J. Phys. Chem. B* **2007**, *111* (33), 9747−9757.

(60)   Amorphous Materials: Properties, Structure, and Durability: Structure of Mg- and Mg/Ca Aluminosilicate Glasses: 27Al NMR and Raman Spectroscopy Investigations . *American Mineralogist* . 2008, p 1721.

(61)   Bhatty, M. S. Y. Crystallization of Anorthite from CaO-Al2O3-SiO2 Glasses. *Mineral. Mag.* **1970**, *37* (291), 780–789.

(62)   Sykes, D.; Kubicki, D, J. Four-Membered Rings in Silica and Aluminosilicate Glasses. *American Mineralogist*. 1996, p 265.

TOC Graphic

SiO$_4$

AlO$_4$

R (=Ca/Mg)

SiO$_4$/AlO$_4$
Network region

R+NBO Channel region

SiO$_4$
Network region

Figure 1: (a) Neutron diffraction structure factors of CMAS glass, experimental data (dots) and RMC simulation (solid black line). (b) Experimental (circles), calculated (continuous line) and difference (continuous line at bottom) X-ray powder diffraction profiles of CMAS-M1 GC. Bragg peaks with vertical bars are indicated for $Ca_2Mg_{0.35}Al_{1.3}Si_{1.35}O_7$, $Ca(Mg_{1-x}Al_x)(Si_{1-x/2}Al_{x/2})_2O_6$, $MgSiO_3$ and $CaSi_2Al_2O_8$ from top to bottom, respectively.

Figure 2: Deconvolution of 29Si NMR spectra of glasses (a) CMAS-M1 and (b) CMAS-M2.
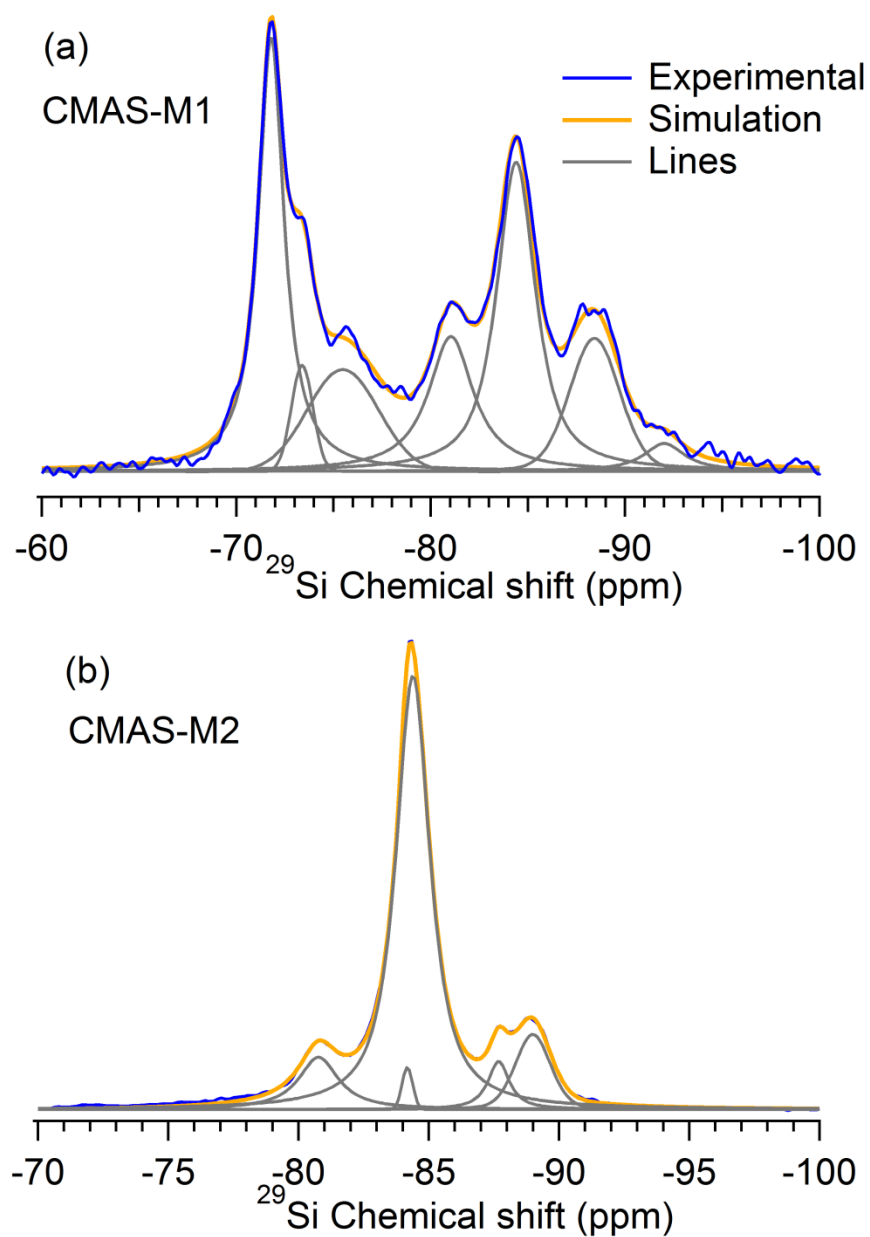
Figure 3: Deconvolution of 29Si MAS NMR spectra of GCs (a) CMAS-M1 and (b) CMAS-M2.
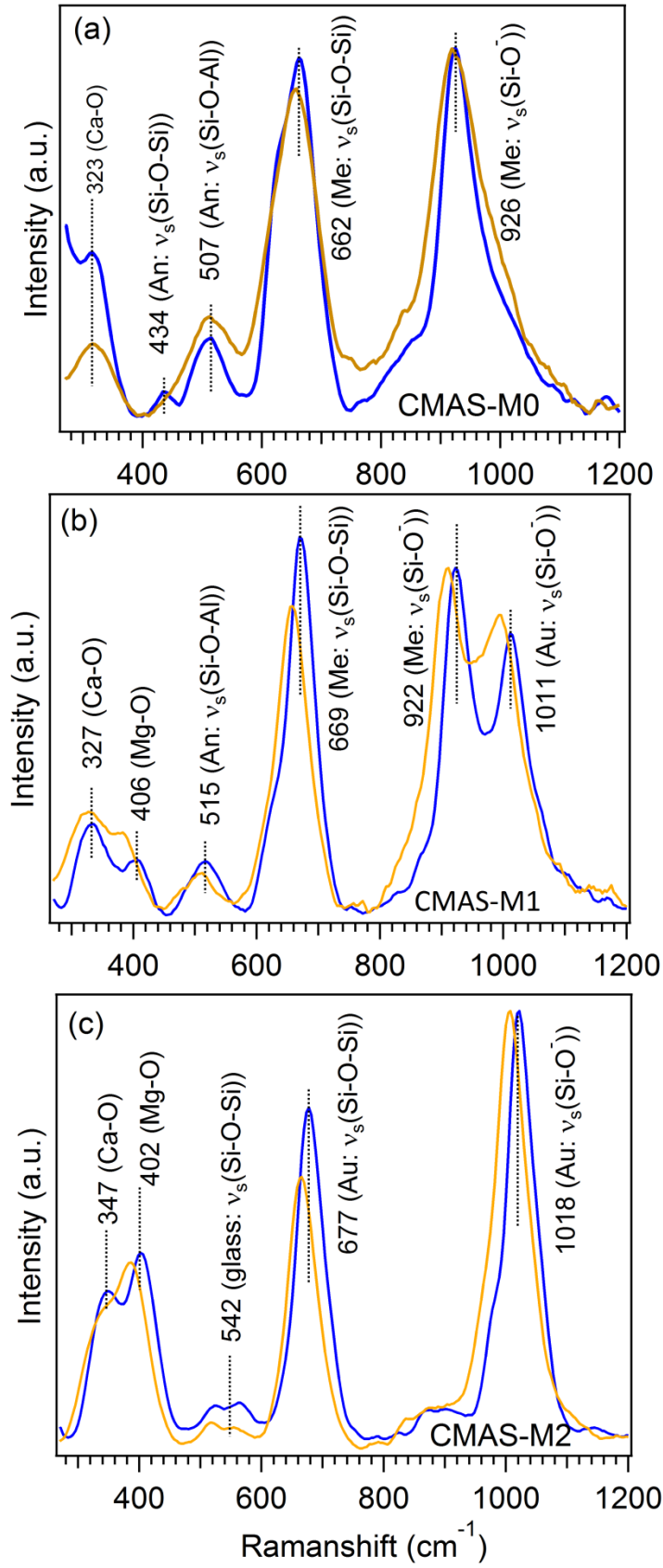
Figure 4: In-situ Raman spectra of (a) CMAS-M0, (b) CMAS-M1, and (c) CMAS-M2 glass-ceramics from room temperature to 800 °C. (Blue lines represent spectra recorded at 100 °C and Brown lines spectra recorded at 800 °C)
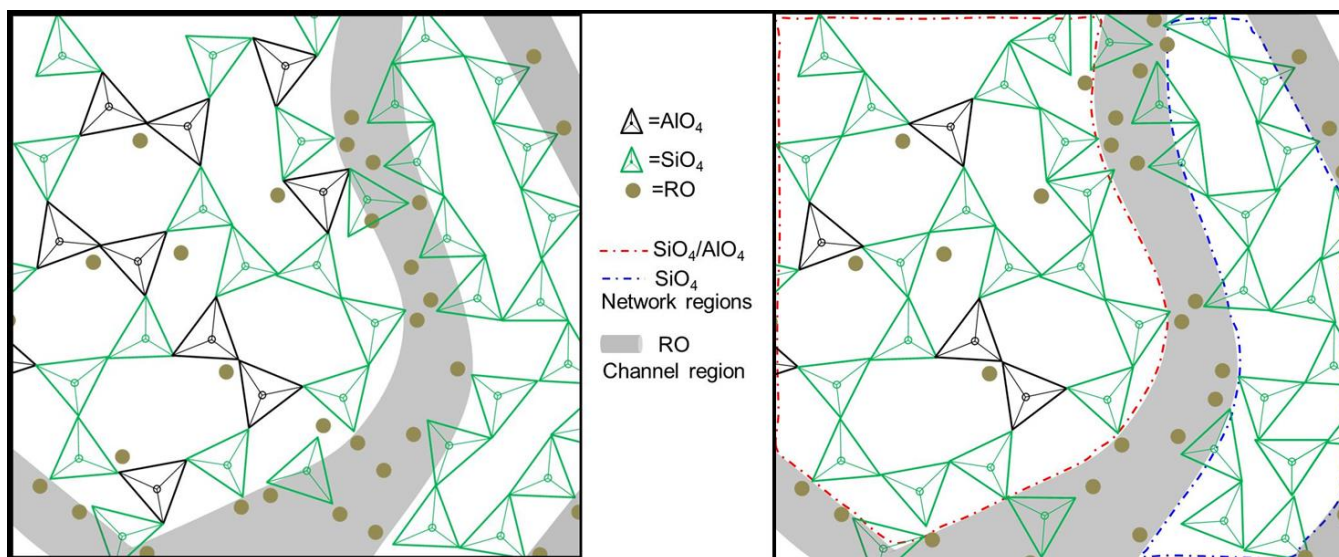
Figure 5: Schematic presentation of possible structural distribution in CMAS-M0 glass (left) and in CMAS-M2 glass (right). In CMAS-M0 glass the fraction of Al-O-Al bonds (black tetrahedral) are larger than in CMAS-M2 glass.